

Dynamics of shallow impact cratering

M.A. Ambroso¹, R.D. Kamien², and D.J. Durian^{1,2}

¹*Department of Physics and Astronomy, University of California, Los Angeles, CA 90095-1547, USA*

²*Department of Physics and Astronomy, University of Pennsylvania, Philadelphia, PA 19104-6396, USA*

(Dated: October 28, 2018)

We present data for the time-dependence of wooden spheres penetrating into a loose non-cohesive packing of glass beads. The stopping time is a factor of three longer than the time d/v_o needed to travel the total penetration distance d at the impact speed v_o . The acceleration decreases monotonically throughout the impact. These kinematics are modelled by a position- and velocity-dependent stopping force that is constrained to reproduce prior observations for the scaling of the penetration depth with the total drop distance.

PACS numbers: 45.70.Ht, 45.70.Cc, 83.80.Fg, 89.75.Da

Granular impact is a phenomenon of natural interest. One focus of recent work is the size and morphology of the crater, and the analogy with planetary cratering [1, 2, 3]. Another is the dramatic splash produced by the collapsing void [4, 5]. Still another is the final depth of penetration, d , because it probes granular mechanics via the depth-averaged stopping force: $\langle F_s \rangle = mgH/d$, where m is the projectile mass, $g = 980 \text{ cm/s}^2$, h is the free-fall distance, and $H = h + d$ is the total drop distance [6, 7, 8, 9, 10]. For shallow impact by spheres [6, 10], and for deeper impacts by cylinders with various tip shapes [7], the penetration depth scales as

$$d/d_o = (H/d_o)^{1/3}, \quad (1)$$

where d_o is the minimum penetration for $h = 0$. The inset of Fig. 1 shows Eq. (1) agreeing with data over nearly three decades in H . While this constrains the stopping force, it does not reveal a unique form. For example, Eq. (1) is equally consistent with $F_s \propto z^2$ and $F_s \propto v^{4/3}$, where z and v respectively are the instantaneous depth and speed of the projectile [6]. Which, if either, of these possible stopping forces is correct? How does the nature of the stopping force, and the resulting transfer of energy from the projectile to the medium, conspire to produce the subsequent granular splash and the final crater morphology? The unintuitive response of granular media to external forcing is a topic of widespread interest beyond the specific example of impact [11, 12, 13].

Recently impact dynamics have been measured by high-speed video [14, 15, 16] and by an embedded accelerometer [17]. In Ref. [14] the total upward force is found to be $\Sigma F = -mg + (mg + kd)$. The stopping force, in parentheses, is independent of time but has a value that depends on the impact speed v_o . Solution of $\Sigma F = ma$ gives a penetration depth of $d = \sqrt{mv_o^2/(2k)}$. In Ref. [15], the total force is found to be $\Sigma F = -mg + k|z|$. The stopping force is Coulomb friction and increases with time. Solution of $\Sigma F = ma$ gives a penetration depth of similar form to Eq. (1): $d/d_o = (H/d_o)^{1/2}$ with $d_o = 2mg/k$. In Refs. [16, 17], the acceleration decreases with time. The various reported force laws thus appear

contradictory, both in terms of their time dependencies and in terms of their predicted penetration depths. Furthermore, none of the reported force laws is consistent with the $d \sim H^{1/3}$ observation of Eq. (1).

In this paper we measure cratering dynamics in the unexplored regime of shallow impact, where the projectile never submerges. Our approach is to measure position vs time with an optical method, both faster and more precise than imaging. Like Refs. [16, 17], we find that the acceleration decreases throughout impact. Our theoretical approach is to consider possible instantaneous force laws whose depth-averages reproduce the observed scaling of Eq. (1). The best candidate depends on both position and speed, and suggests that the seemingly disparate results of Refs. [6, 14, 15, 16, 17] may not be contradictory but instead may represent limiting cases of a common force law that holds for both shallow and deep impacts.

Our materials and penetration depth measurements are identical to those of Ref. [10]. The medium consists of glass beads, diameter $D_g = 0.30 \pm 0.05 \text{ mm}$, prepared at 59% packing fraction by slowly turning off a fluidizing upflow of air. The projectiles are wooden spheres of diameter $D_b = 1.49 \text{ inch}$ or $D_b = 1.99 \text{ inch}$, and of density $\rho_b = 0.7 \text{ g/cc}$. These are held and dropped from rest via a suction mechanism. The drop distance and final penetration depth are measured with a telescope mounted to a height gauge. Data for the wooden spheres of Ref. [10], and for the dynamics runs reported here, are shown in the inset of Fig. 1 to obey Eq. (1).

The time-dependent vertical position of the projectile is measured optically. A laser ($\lambda = 532 \text{ nm}$) is placed about 1.5 m from the sample, along with a cylindrical lens that fans the beam into a thin sheet. An aperture is used to select the central portion of the beam, where the intensity is nearly constant, and to set its size to be slightly greater than D_b . On the other side of the projectile, we align a second aperture equal to D_b . Behind this we place a large planoconvex lens to focus the light onto a photodiode. As such, the collected light intensity varies nearly linearly with projectile position. In each run

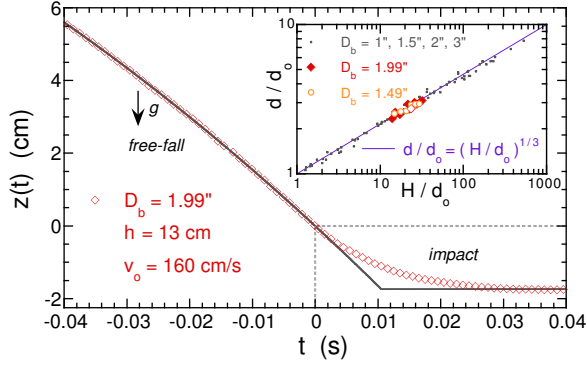


FIG. 1: The vertical position z of the bottom of a sphere vs time t , for typical conditions as labelled. The impact begins at $\{z = 0, t = 0\}$, and gravity points in the $-z$ direction. Only every $1/100^{\text{th}}$ datum is shown. The inset shows the final penetration depth vs total drop distance, both scaled by the minimum penetration depth d_o . The small symbols represent data for four wooden spheres from Ref. [10]. The large symbols represent new runs, for which in this manuscript we report on impact dynamics (\diamond is for the example in the main plot). The values of d_o are 0.63 cm and 0.44 cm for the 1.99 inch and 1.49 inch diameter spheres, respectively.

the photocurrent starts at a maximum, decreases as the projectile freely falls onto the beam, goes to zero when the beam is fully blocked, and then increases as the projectile falls further and light passes over its top; impact occurs during this last phase. To calibrate we hold the ball in several known positions, with light passing above and below, and we fit to the particular cubic polynomial expected for an aligned Gaussian beam.

Typical depth vs time data are displayed in Fig. 1. The impact occurs at $t = 0$, and the projectile comes to rest in about 0.03 s. The solid curve through the $t < 0$ free-fall data is not a fit, but rather $-v_o t - gt^2/2$ with $v_o = \sqrt{2gh}$. We digitized the photocurrent using a 12-bit A/D converter operating at 10^5 points per second. Finer digitization and faster capture could be achieved at marginally greater expense. The fidelity with which impact dynamics can be captured by our method exceeds high-speed video. Notwithstanding, there exist certain limitations. One is that for large enough drop heights the grains splash into the laser beam. A lesser limitation is that the minimum drop height was such that none of the beam was blocked by the projectile prior to its release. Overall we achieved over a factor of two variation in total drop distance for each sphere. To differentiate position vs time data, we fit to a cubic polynomial with Gaussian weighting that nearly vanishes at the edges. For fitting windows that are too small, the velocity and acceleration results are noisy; for fitting windows that are not too large, the depth-averaged acceleration equals gh/d as required by energy conservation. This check gives confidence in both our data and our differentiation procedures.

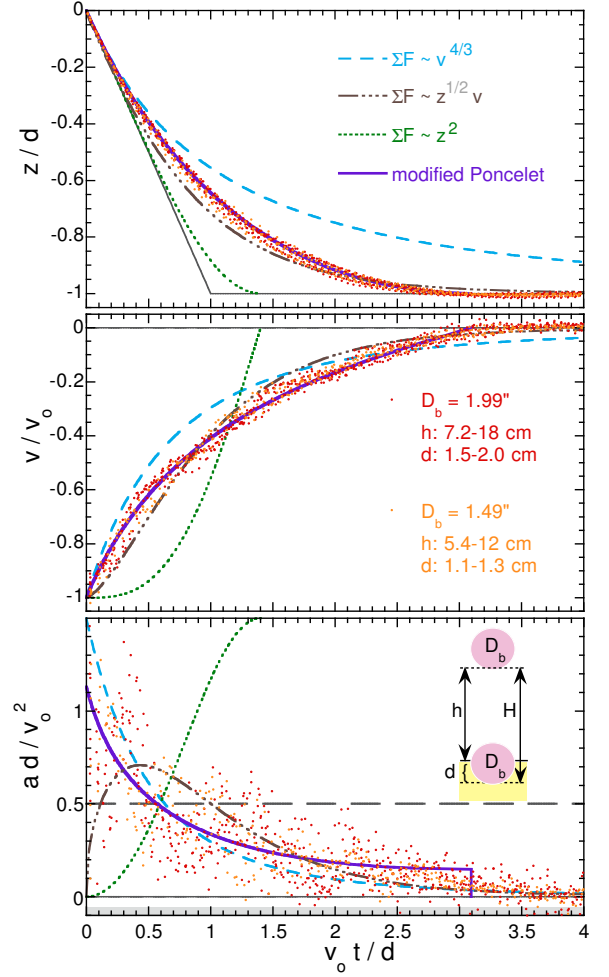


FIG. 2: Vertical components of position, velocity, and acceleration vs time, for all runs; red (orange) dots are for $D_b = 1.99$ inch (1.49 inch). To within measurement errors, the data collapse when lengths are scaled by d and times are scaled by d/v_o , where d is the final penetration depth and v_o is the impact speed. By construction, the scaled position data all decay from 0 to -1 with an initial slope of -1 (gray lines). Note that the acceleration is not constant (gray dashed line $ad/v_o^2 = 1/2$), but rather decreases with time. The data rule out the power-law forces consistent with Eq. (1), but are consistent with a modified Poncelet model.

Data for position-velocity-acceleration vs time, for both spheres and all drop heights, are displayed in Fig. 2. All lengths are scaled by the final penetration depth d , and all times are scaled by the time d/v_o required to move a distance d at the impact speed v_o . To within measurement error, the data all collapse according to this scaling. By construction, the scaled position data must decay from 0 to -1 with an initial slope of -1 ; the scaled-velocity data must decay from -1 to 0; and the depth-average of the scaled acceleration must equal $1/2$. We find that the spheres all come to rest at about $3v_o t/d$, roughly three times longer than if they moved the same distance at constant speed. Since $v_o \sim h^{1/2}$ and $d \sim H^{1/3}$ have

similar scaling, the impact duration is nearly constant as in Refs. [14, 17]. We also find that the acceleration decreases with time, in accord with Refs. [16, 17] but in contrast to Refs. [14, 15]. Note that the scaled value of gravitational acceleration is $-gd/v_o^2 = -d/(2h)$; this ranges from -0.05 to -0.10 for our runs (shaded gray region in Fig. 2c) and is generally small compared to the projectile acceleration.

Our impact dynamics data can now be compared with expectations for various candidate force laws. For example the simple *ad-hoc* form $\Sigma F = -mg + k|z|^\alpha|v|^\beta$ best agrees with Eq. (1) if the exponents are related by $\beta = (4 - 2\alpha)/3$. The agreement becomes exact for $\Sigma F = -mg + k|z|^2$. Predictions for this special case, $\{\alpha = 2, \beta = 0\}$, and also for $\{\alpha = 0, \beta = 4/3\}$, are displayed with the scaled data in Fig. 2. Evidently, the decay of $z(t)$ is too fast for the former and too slow for the latter. The actual behavior lies between these extremes. A marginally-acceptable fit, also shown, is attained for $\{\alpha = 1/2, \beta = 1\}$.

Better fits can be achieved if the stopping force equals a constant plus a term that grows with speed. If the drag is viscous, then the force law is given by the Bingham model, $\Sigma F = -mg + (F_o + b|v|)$. If the drag is inertial, then the force law is given by the Poncelet model, $\Sigma F = -mg + (F_o + cv^2)$. The Bingham model has recently been advocated for granular impact [8], while the Poncelet model has long been used for ballistics applications [18]. For both, position vs speed can be found by writing $a = vdv/dz$, separating variables, and integrating. All our dynamics data are shown again in phase space plots of scaled velocity and acceleration vs depth, as well as acceleration vs speed, in Fig. 3. The best one-parameter fits to these models give $(F_o - mg)/(bv_o) = 0.065$ and $(F_o - mg)/(cv_o^2) = 0.20$, respectively; χ^2 is smaller for the Poncelet model by a factor of two. These fits (not shown) are both acceptable, but not quite as nice as the one displayed. Still, neither model predicts the observed penetration depth scaling of Eq. (1). The Bingham model gives $d = (mv_o/b)[1 - \alpha \ln(1 + 1/\alpha)]$ where $\alpha = (F_o - mg)/(bv_o)$, and the Poncelet model gives $d = [m/(2c)] \ln(1 + 1/\alpha)$ where $\alpha = (F_o - mg)/(cv_o^2)$. Furthermore the predicted initial accelerations, and the final penetration depths, are unphysical in the limit $v_o \rightarrow 0$.

We now modify the Poncelet model along the lines suggested by Tsimring and Volfson [19]. Since the constant term represents friction, it should depend on depth according to hydrostatic pressure [15, 20] and the geometry of the granular medium near the projectile: $\Sigma F = -mg + [F(z) + cv^2]$. For any $F(z)$ this can be recast as an ordinary differential equation for kinetic energy vs position and solved by use of an integrating factor, $\exp(-2cz/m)$. To *exactly* recover the observed penetration depth scaling, Eq. (1), and hence be consistent with the observed depth-averaged stopping force, we find that the friction

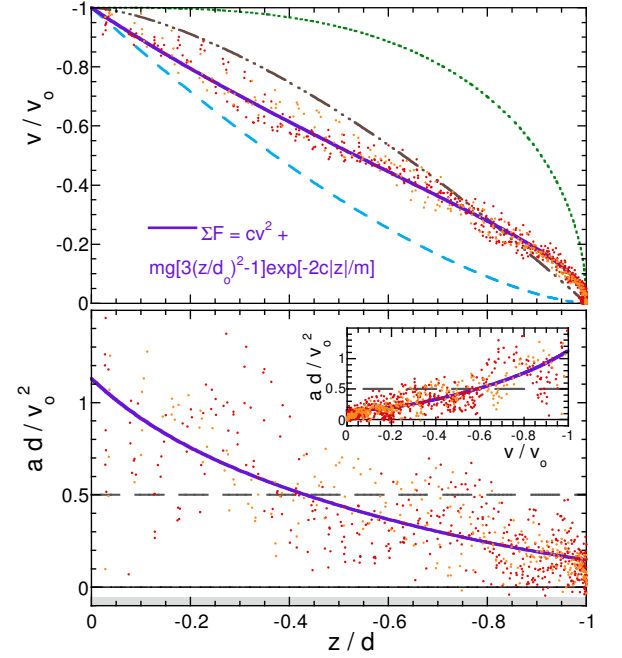


FIG. 3: Velocity and acceleration vs position, and acceleration vs velocity (inset), for all runs, scaled as in Fig. 2; red (orange) dots are for $D_b = 1.99$ inch (1.49 inch). Excellent fits to the modified Poncelet model are shown as solid purple curves. The various-dashed curves represent the same power-law forces as in Fig. 2.

term must be $F(z)/mg = [3(z/d_o)^2 - 1] \exp(-2|z|/d_1) + 1$ where $d_1 = m/c$. This vanishes for shallow penetration and approaches a constant for deep penetration, consistent with the special limits advocated in Ref. [19]. Altogether the projectile acceleration in our model is

$$a/g = [3(z/d_o)^2 - 1] \exp(-2|z|/d_1) + v^2/(gd_1). \quad (2)$$

For high speeds and deep impacts the velocity term dominates. For shallow impacts, the leading behavior is $a/g \approx -1 + 2|z|/d_1 + (3/d_o^2 - 2/d_1^2)z^2 + v^2/(gd_1)$. For zero impact speed, the initial acceleration is $-g$, as expected.

To compare our force model with data, it is convenient to work in phase space since velocity vs depth can be computed directly as

$$\left(\frac{v}{v_o}\right)^2 = \left[1 - \frac{|z/d|^3 - |z/d|(d_o/d)^2}{1 - (d_o/d)^2}\right] e^{-2|z|/d_1}. \quad (3)$$

For $v_o = 0$, the relation is $v^2 = 2gd_o(|z/d_o| - |z/d_o|^3) \exp(-2|z|/d_1)$. Since the predicted dynamics depend on the value of d/d_o , the apparent collapse of data in Fig. 2 would then represent clustering about an average to within measurement error. Setting $d/d_o = 2.77$, the average value for all our runs, the best one-parameter fit to Eq. (3) is for $d/d_1 = 1.2$. This gives an excellent description of the data, as shown by the solid purple curves in Figs. 2-3.

As the ball comes to rest, in all acceptable fits, the time becomes about $3d/v_o$ and the upward acceleration becomes one to two g . After stopping the acceleration abruptly vanishes, as seen directly in measurement by accelerometer [17]. The discontinuity is more apparent here in plots of acceleration vs position or speed (Fig. 3) than in plots of acceleration vs time (Fig. 2c).

In conclusion, we have measured the dynamics of impact to further constrain the form of the force law responsible for prior observations of final penetration depth vs total drop distance, $d \sim H^{1/3}$ [6, 7, 10]. For two sphere sizes, and a factor of two in drop distance, the position vs time data appear to collapse when scaled by impact speed and final depth. Several possible force laws can now be ruled out altogether. Two velocity-dependent force laws are consistent with dynamics but not with penetration depth data. The best candidate is a modification of the Poncelet model along the lines suggested in Ref. [19]. It features inertial drag plus a particular depth-dependent friction term designed to exactly recover the penetration depth scaling of Eq. (1). The predicted kinematics, Eqs. (2-3), agree very well with our new data. The model has two important length scales, the minimum penetration depth d_o and an inertial drag length d_1 . The former is given by $d_o = (0.14/\mu)^{3/2}(\rho_b/\rho_g)^{3/4}D_b$ where μ is the tangent of the repose angle, ρ_g is the grain density, ρ_b is the ball density, and D_b is the ball diameter [10]. For the system examined here, d_1 is about twice as large as d_o but we do not yet know the dependence of d_1 on system properties. This could be deduced, and the model could be further tested, by measurement of impact dynamics over a broad range of conditions. At one extreme, the “dry quick sand” examined in Ref. [15] for $v_o = 0$ is reproduced very well by our model with $d_1 = 3d_o$.

We thank D. Lohse, L.S. Tsimring, and P.B. Umbanhowar for sharing their results prior to publication. We thank T.C. Lubensky and P.T. Korda for helpful discussions. This material is based upon work supported by the National Science Foundation under grant DMR-0305106.

- [2] Y. Grasselli and H. J. Herrmann, *Gran. Matt.* **3**, 201 (2001).
- [3] A. M. Walsh, K. E. Holloway, P. Habdas, and J. R. de Bruyn, *Phys. Rev. Lett.* **91**, 104301 (2003).
- [4] S. T. Thoroddsen and A. Q. Shen, *Phys. Fluids* **13**, 4 (2001).
- [5] D. Lohse, R. Bergmann, R. Mikkelsen, C. Zeilstra, D. van der Meer, M. Versluis, K. van der Weele, M. van der Hoef, and H. Kuipers, *Phys. Rev. Lett.* **93**, 198003 (2004).
- [6] J. S. Uehara, M. A. Ambroso, R. P. Ojha, and D. J. Durian, *Phys. Rev. Lett.* **90**, 194301 (2003), and erratum **91**, 149902 (2003).
- [7] K. A. Newhall and D. J. Durian, *Phys. Rev. E* **68**, 060301R (2003).
- [8] J. R. de Bruyn and A. M. Walsh, *Can. J. Phys.* **82**, 439 (2004).
- [9] X.-J. Zheng, Z.-T. Wang, and Z.-G. Qiu, *European Physical Journal E* **13**, 321 (2004).
- [10] M. A. Ambroso, C. R. Santore, A. R. Abate, and D. J. Durian (2004), cond-mat/0411231.
- [11] R. L. Brown and J. C. Richards, *Principles of Powder Mechanics* (Pergamon Press, Oxford, 1970).
- [12] H. M. Jaeger, S. R. Nagel, and R. P. Behringer, *Rev. Mod. Phys.* **68**, 1259 (1996).
- [13] J. Duran, *Sands, powders, and grains: An introduction to the physics of granular materials* (Springer, NY, 2000).
- [14] M. P. Ciamarra, A. H. Lara, A. T. Lee, D. I. Goldman, I. Vishik, and H. L. Swinney, *Phys. Rev. Lett.* **92**, 194301 (2004).
- [15] D. Lohse, R. Rauhe, R. Bergmann, and D. van der Meer, *Nature* **432**, 689 (2004).
- [16] K. E. Daniels, J. E. Coppock, and R. P. Behringer, *Chaos* **14**, S4 (2004).
- [17] P. B. Umbanhowar (2004), private communication.
- [18] M. E. Backman and W. Goldsmith, *International Journal of Engineering Science* **16**, 1 (1978).
- [19] L. S. Tsimring and D. Volfson, preprint (2005), submitted to *Powders and Grains 2005*.
- [20] I. Albert, J. G. Sample, A. J. Morss, S. Rajagopalan, A. L. Barabasi, and P. Schiffer, *Phys. Rev. E* **64**, 061303 (2001), and references therein.

[1] J. C. Amato and R. E. Williams, *Am. J. Phys.* **66**, 141 (1998).